

High-Performance Reactionless Scan Mechanism

Ellen I. Williams*, Richard T. Summers* and Miroslaw A. Ostaszewski**

Abstract

A high-performance reactionless scan mirror mechanism was developed for space applications to provide thermal images of the Earth. The design incorporates a unique mechanical means of providing reactionless operation that also minimizes weight, mechanical resonance operation to minimize power, combined use of a single optical encoder to sense coarse and fine angular position, and a new kinematic mount of the mirror. A flex pivot hardware failure and current project status are discussed.

1.0 Introduction

The reactionless scanning mechanism replaces the earlier mechanisms designed to map thermal radiation from the Earth with the goal of weighing less and having higher performance. Built by Ball Corporation, Aerospace Systems Division, the new scanner system consists of the scanning mechanism and the servo drive electronics (Figure 1).

2.0 Mechanical Description

2.1 General Description. The reactionless scanning mechanism is comprised of two legs, the Encoder Side Assembly (ESA) and the Flex Lead Side Assembly (FLSA), that support a yoke assembly mounted on bearings for coarse angular travel. Coarse angular travel is accomplished using a stepper motor. The mirror/mirror carrier (MMC) and reaction mass (RM) assemblies are within the yoke assembly. The MMC and RM assemblies are mounted on flexures to allow for fine angular travel over the scanning angle range. Scanning motion is accomplished using linear actuators mounted between the RM and the yoke assemblies. RM motion is transferred to the MMC through drive flexures that tie the two assemblies together. These drive flexures allow for out-of-phase motion of the two masses, which effectively cancels any generated forces and torques. During scanning, a brake is used to secure the yoke assembly. Angular position information for both the coarse and fine travel is obtained from an optical encoder referenced to one of the support legs (Figure 2).

The scanning mechanism is servo controlled by the control electronics that are mounted separately in an electronics box. The control electronics house the power supply, optical encoder processing electronics, servo electronics, and command and telemetry interface electronics. The control electronics operate from a 28 Vdc power bus.

2.2 Reactionless Scanner. The scanning assembly is contained within a yoke assembly. It consists of the mirror, the kinematic mounts for the mirror, the mirror

* Ball Corporation, Aerospace Systems Division, Boulder, CO

** former employee of Ball Corporation, Aerospace Systems Division

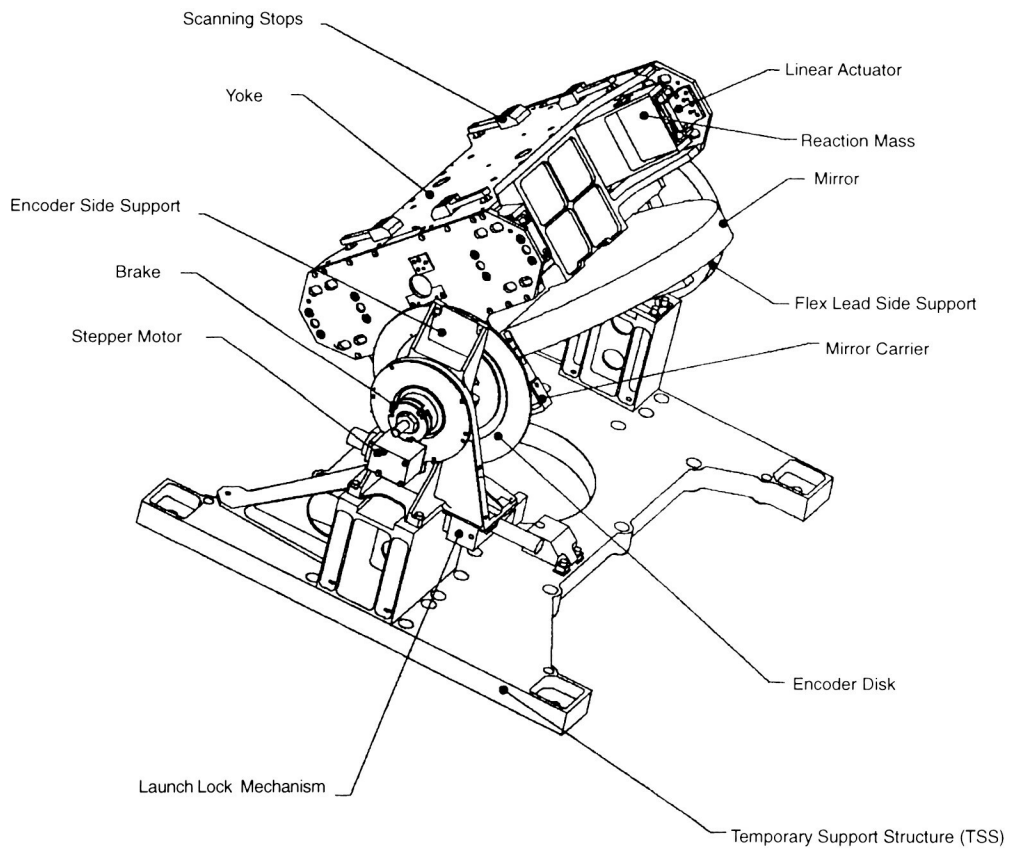
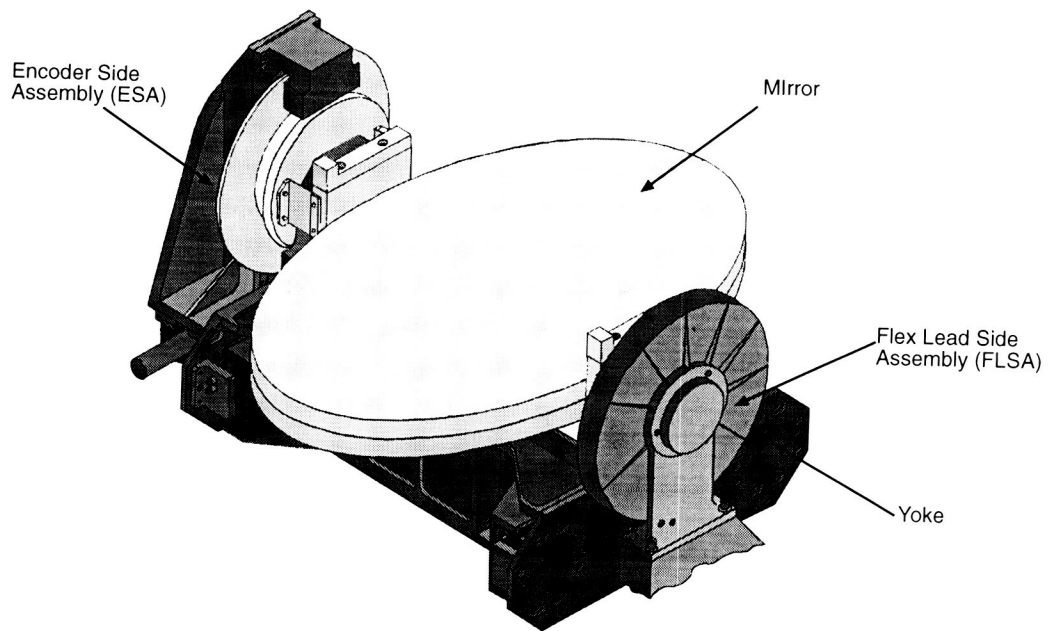


Figure 1. Reactionless scanner assembly, front and back views

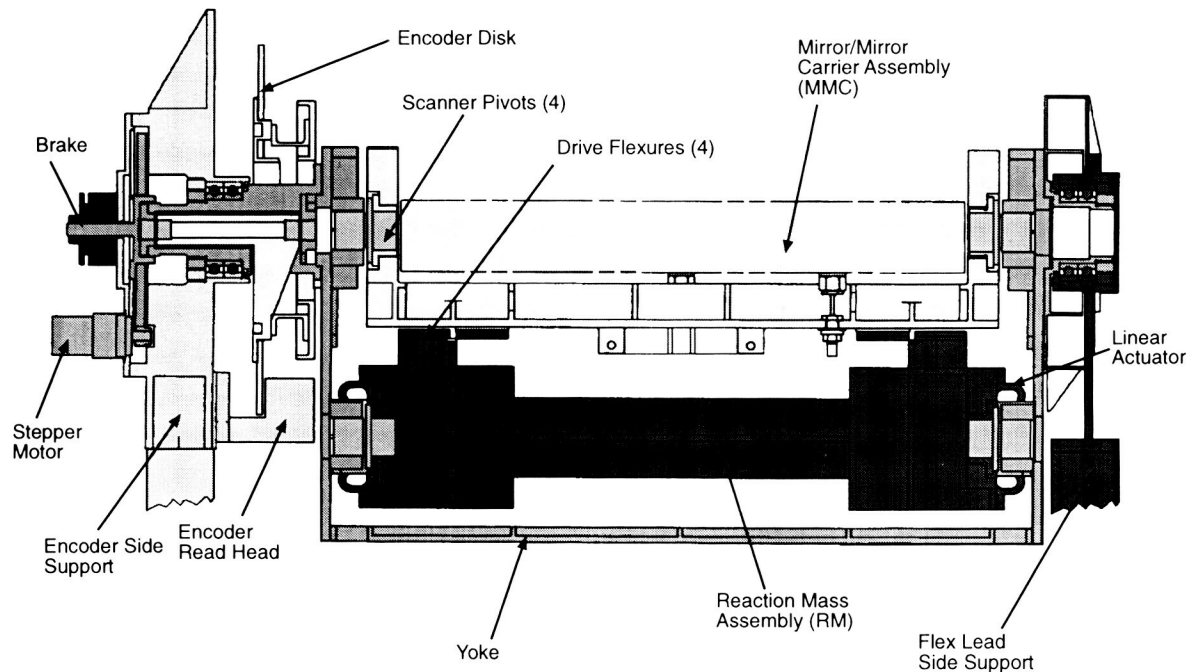


Figure 2. Reactionless scanner section

carrier, the reaction mass, the drive flexures, and the linear actuators (Figure 3).

The Mirror. The scanner system must be able to accommodate a 277.9 x 441.7 mm elliptical flat mirror with an aperture of $\geq 267.18 \times 433.1$ mm. The system aligns the pivot axis 15 mm behind the mirror surface and parallel to the minor axis of the ellipse within 0.05 mm. The mirror flatness must be maintained within 0.4 μm peak to valley and have a slope angle of less than 0.65 arc second over a broad range of thermal influences while subjected to high scanning torques. The surface roughness must be less than 0.005 μm_{RMS} .

The mirror has two halves, 17.53 mm thick each, of I-70 beryllium that are pocketed out to have a ribbed light-weighted structure. The two halves are brazed together, mounted on the back with kinematic mounts, and polished and coated for final performance. The coating of the mirror is a vacuum deposited gold with a specialized overcoat.

The Mirror Carrier. The MC is made from structural grade beryllium, S-200F, that provides the three-point kinematic mount for the mirror, the mounting for the driving flexures, and the pivot flexures for the scanning motion.

The kinematic mounts have two flexing elements account for the thermal growth differences of the structures. Figure 4 depicts the kinematic mounts. The Y-Flexure mount accommodates differential growth in the direction of the major axis of the mirror. The XY Stabilizer Post accommodates change in the minor and major axis plane of the mirror. The Post Mount is a stiff mount that does not flex. At two locations, the Y-

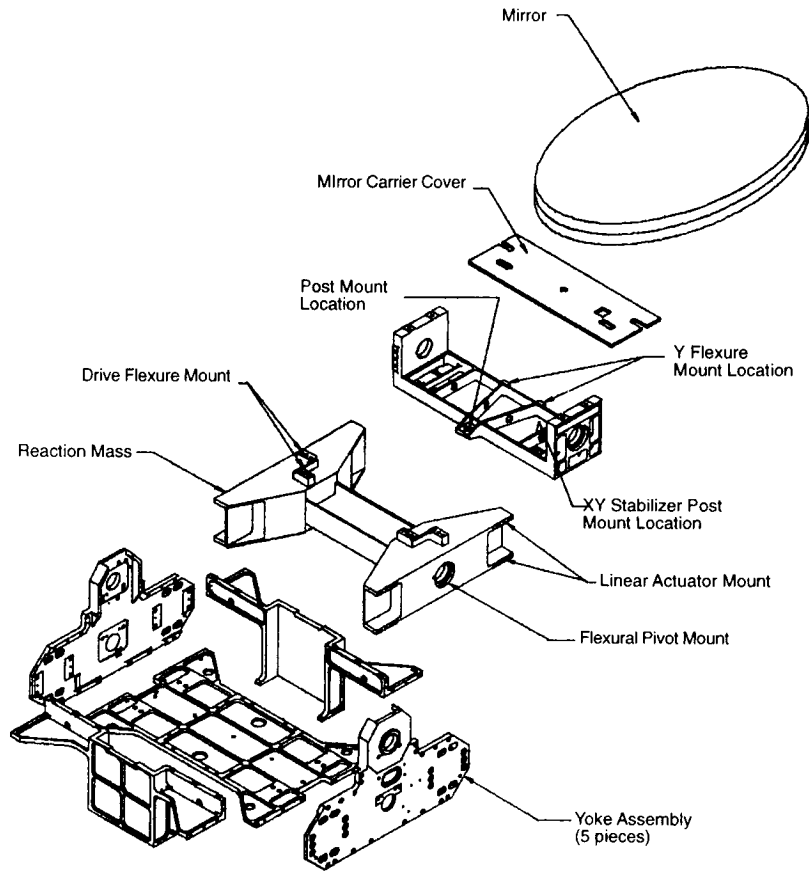


Figure 3. Reactionless Scanner

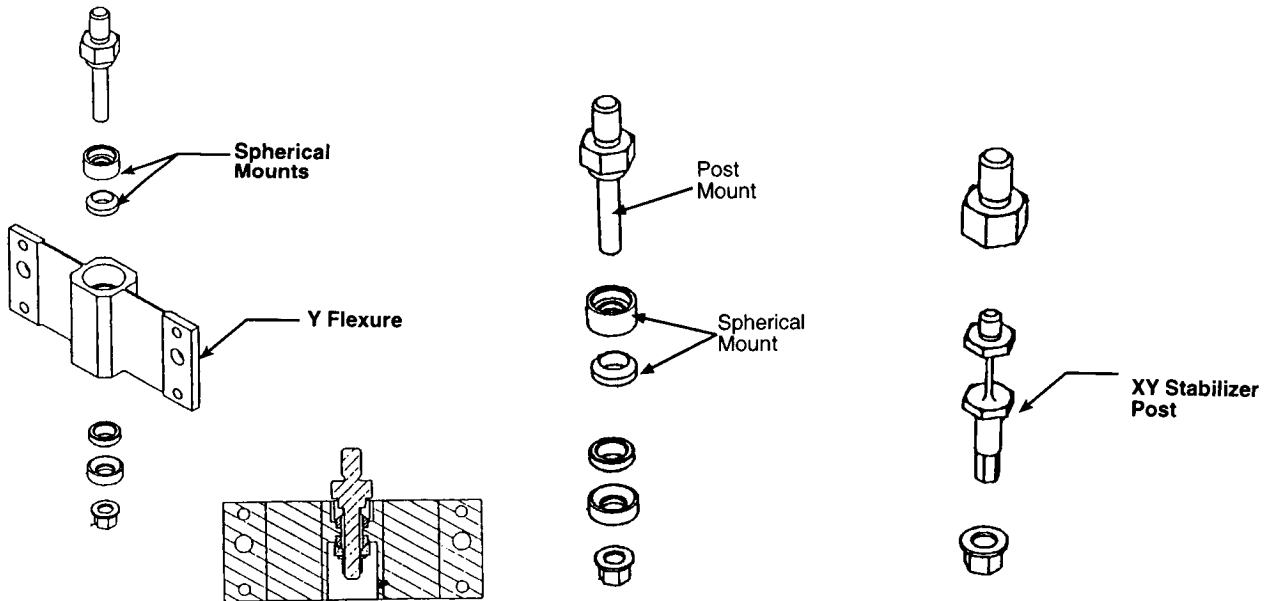


Figure 4. Kinematic Mirror Mounts

Flexure and the Post Mount, a spherical mount is included that accommodates alignment motion during assembly and is then torqued to levels that do not allow the spherical mount to move.

The Reaction Mass. During the scanning operation the RM moves in opposite angular motion to counteract the forces generated due to the MMC action. It also provides the mount for the linear actuators, the driving flexures, and an independent pivot axis (from the mirror scanning axis). Thermal effects from the actuator coils are also kept at a maximum distance from the mirror.

The RM structure consists of an I-beam crossbar that has two symmetrical members brazed to the ends. All the members of the RM are made from structural grade beryllium, S-200F. The I-beam is designed torsionally flexible. The two end members are stiff and place the linear actuators at a location that uses the linear actuator weight as an inertia match for the MMC thereby minimizing weight of the system.

The Drive Flexures. The MC and the RM are connected through a set of four drive flexures that behave as a set of frictionless gears. The drive flexures cause the two assemblies to rotate out of phase without backlash, hysteresis, rubbing or sliding elements, and associated reliability and contamination concerns. This design requires no lubrication.

All four drive flexures are identical and mounted in pairs with one in an 180 deg opposite orientation as shown in Figure 5. The flexure is an assembly of a titanium flexing blade with four mounting blocks. It is designed for 1.75 deg maximum deformation at each end and is designed for infinite fatigue life.

The Linear Actuators. The actuators consist of four efficient magnet/core structures mounted directly to the RM on equal moment arms. They are designed to input torque moments into the system with limited residual forces. The actuators are part of the RM and are closely integrated with the design of the RM itself. The stiffness, power, and weight requirements required optimization of physical size, weight, mounting radius, and motor constant to achieve the requirements. In addition, high reliability is an

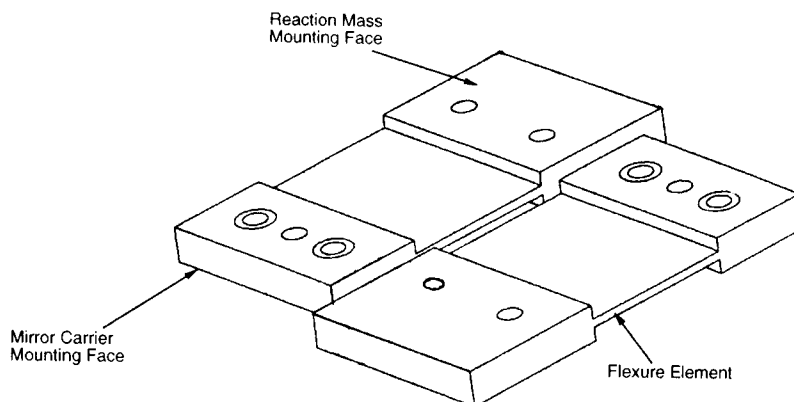


Figure 5. Drive Flexures

important design driver. The motor coils are mounted to the yoke so there is no direct conduction heat path to the mirror, and there are no moving leads. The reaction mass itself provides a shield against motor thermal radiation to the mirror's back surface.

The Flex Pivots. The MC and the RM are individually supported by flex pivots. The pivots must be designed to support all the loads developed during launch. These loads are considerable and are a major design driver. Each assembly has two flex pivots that create a pivot axis for the RM and a pivot axis for the MC. Flex pivots are a system of cross-bladed flexing elements that provide frictionless, lubrication free, and low hysteresis bearing with high radial and axial stiffness. The torsional stiffness was designed to optimize the power requirements.

The flex pivots are commercially made but have been available since the mid-1960's [1]. The standard commercial assembly, shown in Figure 6, consists of an outer cylindrical housing, an inner cylindrical housing, and three flex blades. During assembly, the blades are electron beam welded into the inner housing and the inner housing is electron beam welded into the outer housing. The outer housing is slotted to have a diametrical gap separating two outer cylinders. These two cylinders are then able to rotate relative to each other in opposite directions. The flex pivots that were produced for this project were customized for mounting interface, torsional spring rate, concentricity, radial stiffness, infinite life, and load carrying capability. The resulting pivot design incorporated a flange mount, a stiffer housing, and four blades oriented at 60 deg instead of 90 deg.

The blade material was changed from the standard 420 SS to 422 SS to improve fatigue life.

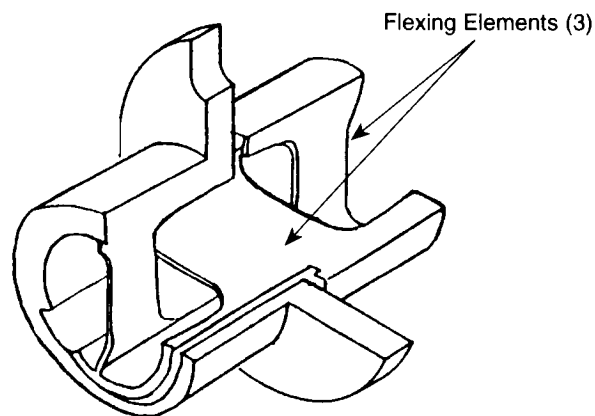


Figure 6. Flexural Pivots

The Yoke Assembly. The yoke assembly is a five-sided structure that contains the RM and MMC assemblies. The outer ends of the flex pivots that support the RM and the MC are mounted on the yoke assembly. The linear actuator coils are also mounted to the yoke assembly, thereby providing a heat path away from the mirror and also eliminating the need for electrical flex leads or bushings for the scanning operation.

The five panels for the yoke assembly are made of structural grade beryllium, S-200F. After initial assembly the final critical surfaces are machined including the bores for the flex pivots, 4 places, and the mounting surfaces and bosses for the support shafts.

2.3 Flex Lead Side Assembly. The FLSA provides support for one half of the yoke assembly, contains the coarse angular travel bearings, houses the flex leads, and is axially compliant to compensate for material thermal differential between the satellite bulkhead and the scanner mechanism (Figure 7).

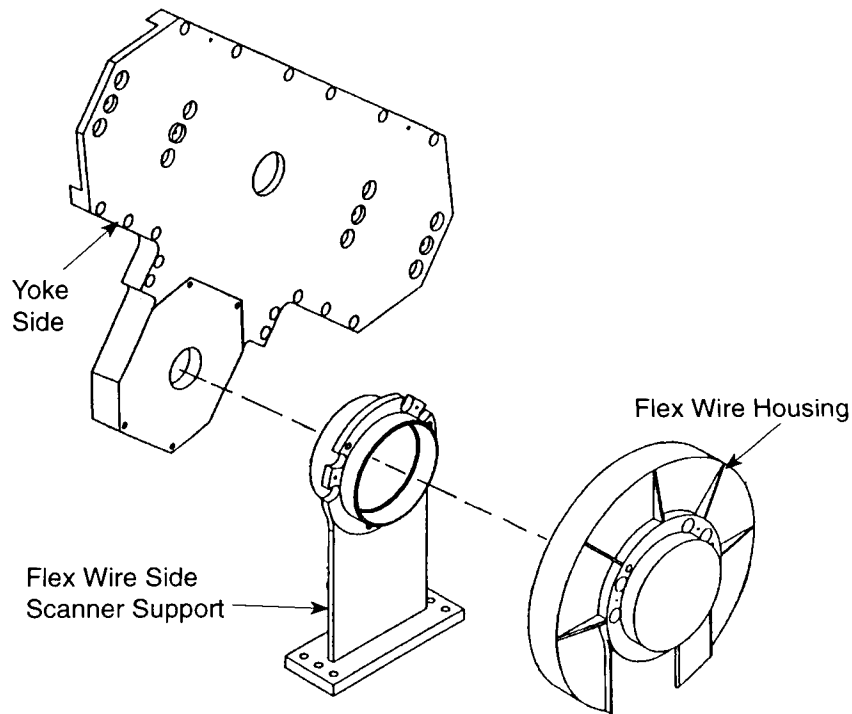


Figure 7. Flex Lead Side Support

There are four twisted shielded pairs (one for each linear actuator) and four thermistor wires that are routed from the yoke assembly to the FLSA. The flex lead housing provides 240 deg freedom of rotation for the flex lead ribbons.

2.4 Encoder Side Assembly. The ESA is the main support for half of the yoke assembly, the coarse angular travel bearings, the drive gear and stepper motor for coarse angular travel, the brake, the encoder disk and spindle, the encoder read head, and the launch lock mechanism (Figure 8).

The Drive Gear and Stepper Motor. The drive gear and the stepper motor drive the yoke assembly through 235 deg for coarse angular travel. The drive gear, made from titanium, has a slot integrated with a pin stop in the support to provide a known location stop at either ends of travel for the electronics servo control. The stepper motor is an Astro Instruments Corporation motor and provides system angular travel at a rate of 0.068 rad/s and requires less than 5 W.

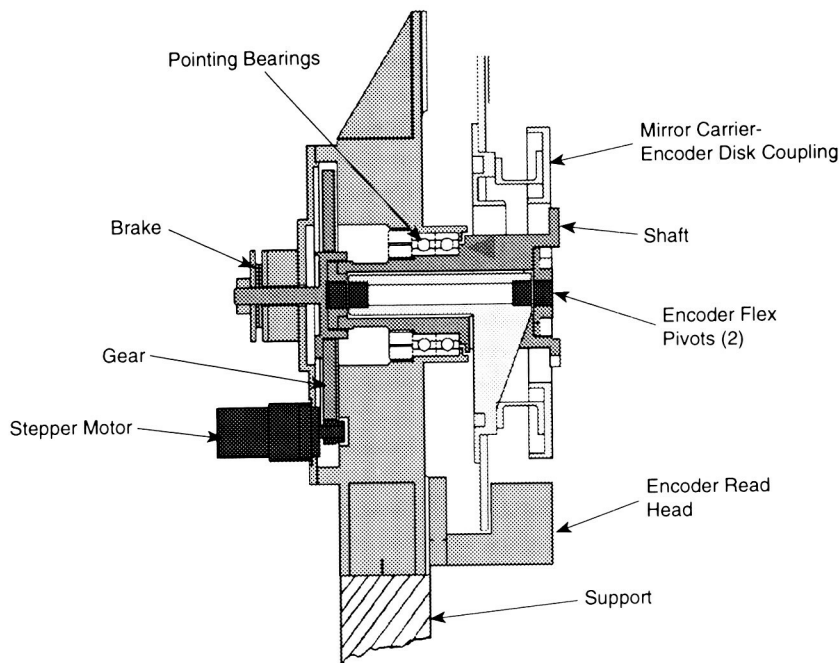


Figure 8. Encoder Side Assembly

The Brake. The brake is designed to hold the yoke assembly in zero gravity once the yoke is in position. It does not stop the yoke assembly during pointing operation (this is controlled by the stepper motor positioning). Due to low out-gassing, material control, low power requirements, and other aerospace design requirements, Ball is designing a brake for the system.

The Encoder Disk, Spindle, and Read Head. The mirror must be positioned during fast scan operation and also coarse pointed for calibration and launch lock. The mirror position must be known throughout the entire range of motion with a specified precision. The encoder is a $1.36 \mu\text{rad}$ per step encoder with the disk, read head, and electronic control board procured from Aerospace Controls Corporation and then mounted and calibrated on Ball parts. The disk is mounted on a spindle that is supported by flex pivots similar to but smaller than the flex pivots used for the MC and RM. The spindle is interconnected to the MC through an inverted box flexure coupling. The coupling allows transmission of MMC torsional motion, but isolates the encoder disk from translational motion. The read head is mounted directly to the support.

The Launch Lock Mechanism. The scanner mechanism is unbalanced and would rotate freely during launch, possibly damaging scanner components. The launch lock, designed by Starsys Research, consists of a paraffin actuator pin-puller that restrains the scanner rotationally during launch. A line-to-line contact is established between the launch lock pin and a feature on the yoke. The pin restrains the yoke in one direction while a feature on the launch lock body restrains it in the other direction. A small gap is allowed to prevent jamming during actuation.

In addition to the launch lock mechanism, snubbers are mounted to the yoke that prevent excessive structural deflection during launch along the rotation axis, which could damage the encoder. The high accuracy requirement for the encoder necessitate close mechanical tolerances between the read heads and encoder disk.

2.5 Reactionless Concept. Figure 9 shows the section view of the scanner and the components that make up the reactionless scanner mechanism. As previously described the MMC and the RM are mounted to the yoke assembly through flex pivots and interconnect to each other through drive flexures. The purpose of the drive flexures is to provide a frictionless gearing system between the RM and the MMC. As the RM rotates in one direction it pulls the MMC through the drive flexures causing the MMC to rotate in the opposite direction. The RM has two sets of linear actuators mounted outboard of the RM. If the rotational inertia of the MMC and the RM are equal and the drive flexures are centered between the two flex pivots, the scanner will operate without any reactions even though the actuators push on the yoke. Of course, this is only true if all the structure, including radial stiffness of the flex pivots, has infinite stiffness. In a real mechanism with mechanical tolerances and structural modes, reactions are generated. Therefore, a critical design goal is to increase the structure stiffness as much as possible which will minimize reactions as well as permit the design of a high servo bandwidth system to control the precision linear scan profile.

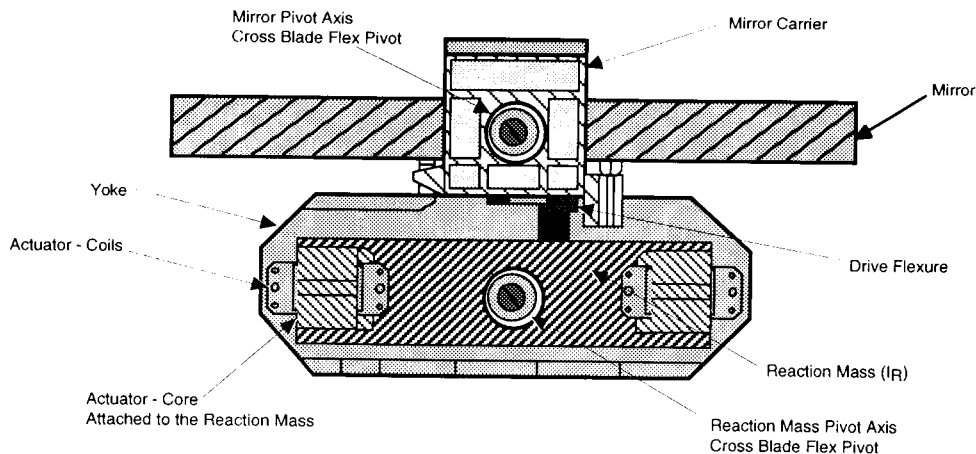


Figure 9. Reactionless Scanner Concept

2.6 Resonance Operation. As the flex pivot torsional stiffness is increased, the rotational natural frequency of the MMC and the RM will increase. The MMC and RM will oscillate sinusoidally when set in motion at a frequency determined by the torsional stiffness of the flex pivots and the rotational inertias of MMC and RM. If the desired scan profile is also sinusoidal, one could exactly match the mechanical natural frequency to the scan frequency. Once the system is set in motion, little power would be necessary to maintain the scan profile. Since the actual scan profile is nearly sinusoidal, an optimum mechanical natural frequency can be determined. Figure 10 shows a graph of computed power vs. scanner natural frequency. From the graph, the minimum power required is when the system mechanical natural frequency is 9.5 Hz.

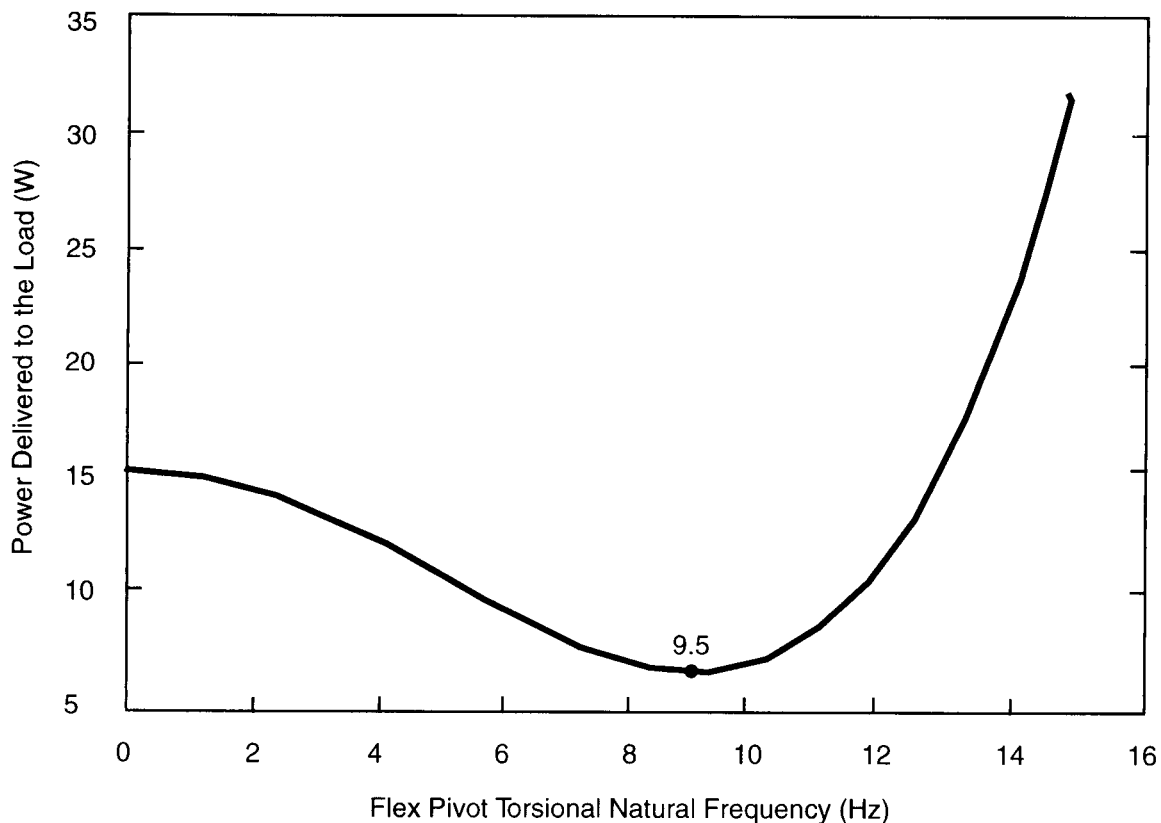


Figure 10. Mechanical Resonance Of $f_n = 9.5$ Hz Is Optimum for the Application Scan Profile

3.0 Performance Design Goals

3.1 Performance Overview. All of the individual pieces and subassemblies were designed to meet a ≥ 500 -Hz first mode resonance. The system must be able to scan the mirror with a flyback pulse and maintain an accurate positional readout. The mirror coarse points in a nominal nadir region and over 90° to a calibration position.

3.2 Mirror. The scanner may not have more than $6.4\text{-}\mu\text{rad}$ angular jitter. The polished, coated mirror is required to exhibit a nominal surface roughness of less than 50 \AA and maintain a minimum reflectance of 98 percent in the 8 to $12\text{-}\mu\text{m}$ band at a 45-deg incident angle over an orbital lifetime of 5 years.

3.3 Scan Profile. Figure 11 shows the required scan profile of the mirror. The mirror must execute a linear scan profile within an angular range of $\pm 1.71 \text{ deg}$ (mechanical angles) with a desired precision of $\pm 15.0 \mu\text{rad}$ (3σ) after 60 sec of observation mode initiation. Linear scan rate is required to be constant to within ± 0.082 percent. Following the linear scan, the mirror executes a non-precision fast fly back. The total scan period will be 0.131 sec (scan cycle frequency will be 7.6 Hz).

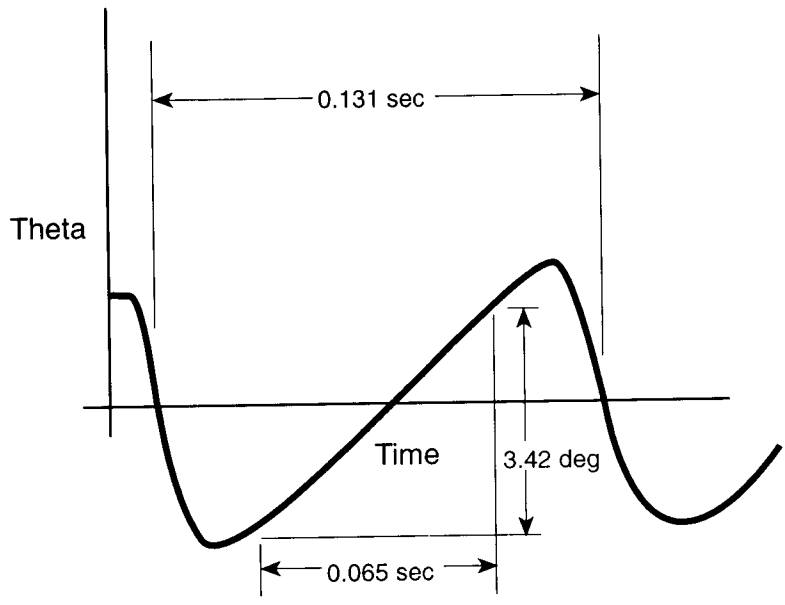


Figure 11. Scan Profile

3.4 Pointing Requirements. The mechanism must be able to adjust the scan position within a ± 4.39 deg (mechanical angle) nominal range with a 0.00549 deg resolution. Also, to calibrate the system, the mirror must be able to rotate 90 deg from the nominal scan position to view a calibration black body. To launch the system, the mirror must rotate -135 deg. Therefore, the total angular travel of the mirror must be 225 deg (Figure 12).

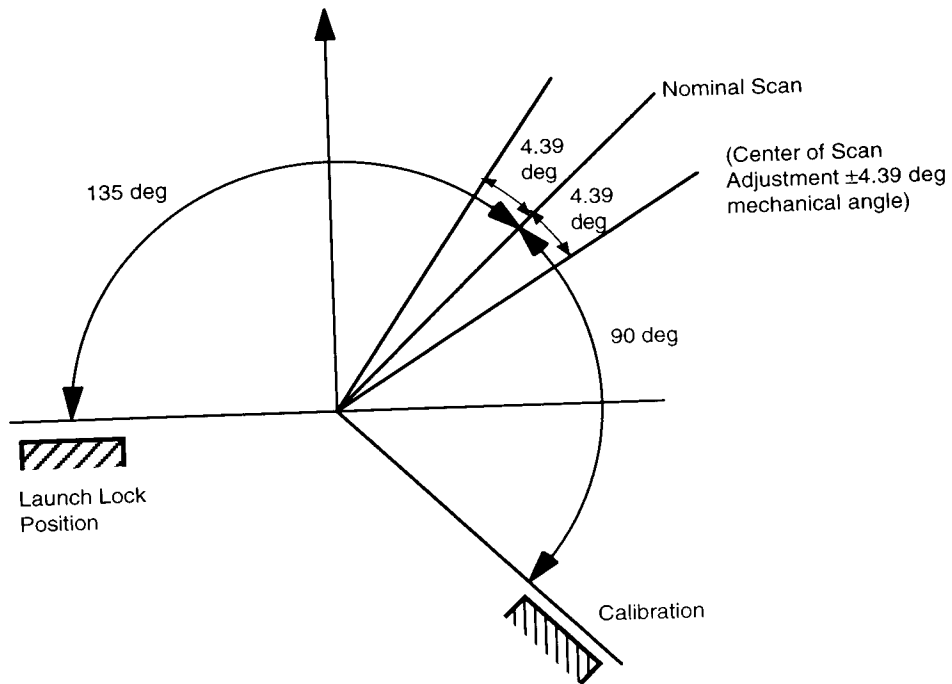


Figure 12. Pointing Range

3.5 Reaction Disturbances. In order for the scanner not to disturb other instruments on the spacecraft, the scanner must operate with minimum reactions.

The rms force disturbance for any one axis for a bandpass of 1 Hz shall not exceed $0.2 N_{RMS}$ over the frequency range of 1 to 40 Hz and $0.13 N_{RMS}$ over the frequency range of 40 to 50 Hz. The total rms force over the frequency range of 1 to 50 Hz shall be less than or equal to $0.4 N_{RMS}$. The power spectral density, PSD, for force disturbance is shown in Figure 13. Force disturbances shall be measured to 150 Hz.

The rms torque disturbance for any one axis for a bandpass of 1 Hz shall not exceed $0.01 Nm_{RMS}$ over the frequency range of 1 to 50 Hz shall be less than or equal to $0.02 Nm_{RMS}$. The PSD for torque disturbance is shown in Figure 14. Torque disturbances shall be measured to 150 Hz. The impulse torque response as a result of stepper motor operation shall not exceed $0.038 Nms_{RMS}$ for a 10 second period.

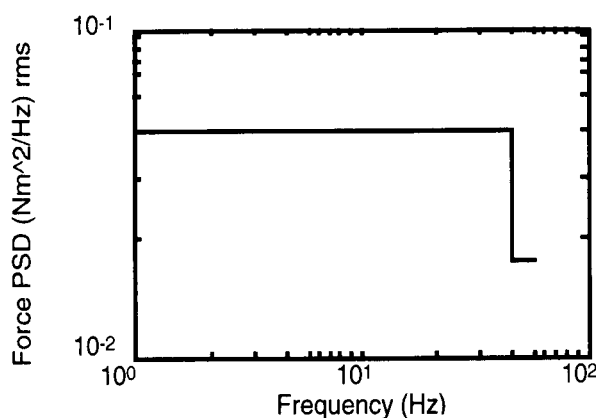


Figure 13. Force Disturbance PSD

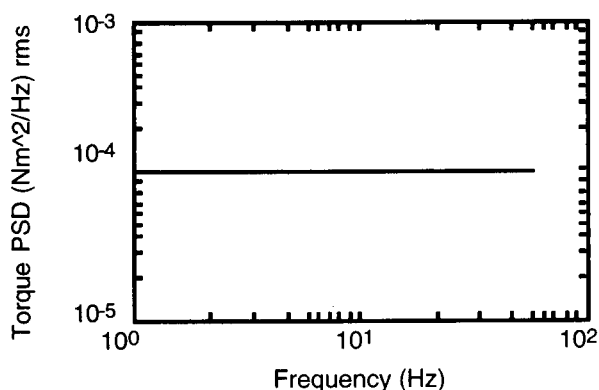


Figure 14. Torque Disturbance PSD

3.6 Mass and Power. The total mass goal for the scanner, including electronics is less than 17.8 kg. Also, the total design power necessary to drive the scanner must be maintained below 30 W rms.

4.0 Flex Pivot Failure

A technical issue that required considerable effort to resolve was the failure of the flexural pivots during random vibration testing. The following is a discussion of the failure, the failure investigation, and the corrective action.

4.1 Hardware Failure. A visual inspection following a $15 G_{RMS}$ Z-axis random vibration test of a prototype scanner revealed the outer blades of the flex pivots were cracked. Figure 15 shows a representative crack. The accelerometer data show that the initial failure occurred about 28 seconds into the test after full vibration level was achieved. The curves show that half-level random ($7.5 G_{RMS}$) produced no damage since there was not marked change in the frequency response from the scanner.

4.2 Failure Investigation and Analysis. The unit was disassembled and all of the pivots were inspected, showing that 12 of 16 scanner flex pivots cracked and 2 of 6 encoder mount flex pivots cracked and buckled. The pivots were sectioned (axially and longitudinally), micrographed, penetrant inspected, and hardness tested. A complete fractography was not possible due to damage of the fracture surface subsequent to failure. All failures occurred at the weld roots (typically the area of low strength). Sections of the weld showed porosity, inclusions, and lack of penetration. Figure 16 displays a prominent void in the weld and Figure 17 shows the weld penetration. Close inspection of the manufacturer's processes revealed potential problems in piece part cleanliness and weld consistency. Another source for weld integrity problems might have been the use of different material for the housing (420 SS) and the blades (422 SS).

The initial scanner NASTRAN model incorporated the pivots as uncoupled springs using manufacturer's data for material strengths, static load carrying capability and spring rate. This model indicated an acceptable margin of safety. The failure created the need for a highly detailed model of the flex pivot.

The overall scanner model incorporated the new detailed flex pivot model to determine the loads generated during random vibration. In addition, sample pivot material was tensile tested. The results indicated strength properties lower than originally believed. The results of the analytical model indicated a negative margin of safety of -0.05 for the flex pivots based on a worst case combination of loads and reduced strength properties. The aforementioned welding flaws compounded the negative margin of safety. The analysis results confirmed the test failure.

4.3 Corrective Action. Multiple paths to improve pivot performance were pursued to be used for the subsequent assemblies. The paths consisted of:

1. Modify the commercial design and processes to produce an acceptable pivot. Ball reworked the manufacturers' design to widen the weld base and reconfigure the blades to use the same housing and blade material. The manufacturer worked with Ball to improve their welding processes. Pivots were lengthened to accommodate weld samples from each pivot and tests were performed on each weld.
2. Negotiate with the customer to reduce the required vibration levels. Past experience has shown that as vibration envelope specifications flow down through multiple levels of contracts, margins often get added onto margins until the specification is difficult to achieve. Negotiations to review the original specification were worked with the customer.
3. Perform rigorous testing and establish selection criteria. Original testing was performed on inadequate fixtures. New fixtures were designed by Ball to provide adequate stiffness and precision.

Tests similar to those outlined by J.L. Olson of Hughes Aircraft Co. [2] are now performed at Ball using the latest technology. The following pivot characteristics are measured: radial stiffness, axial stiffness, torsional spring rate and geometric

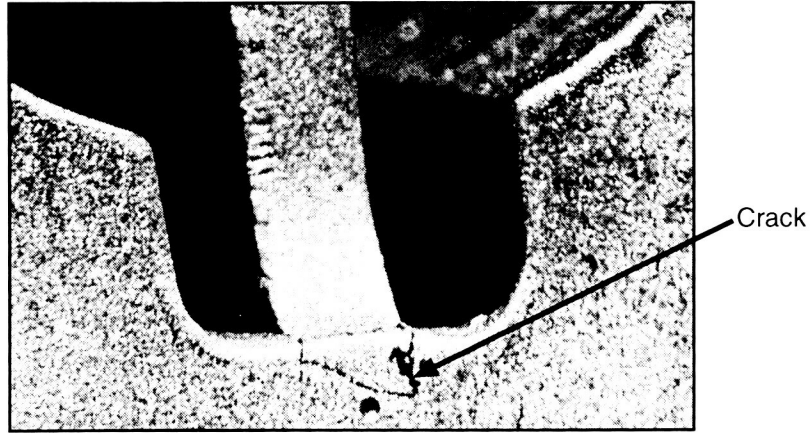


Figure 15. Representative Crack

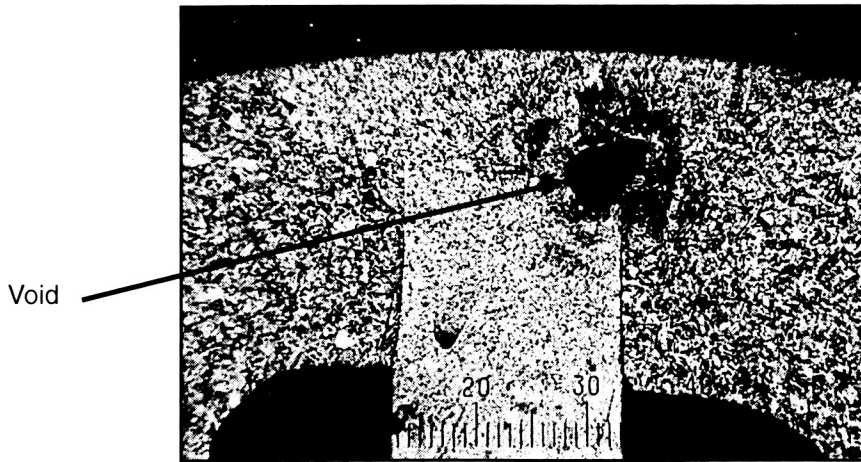


Figure 16. Weld Zone Along Crack (30X)

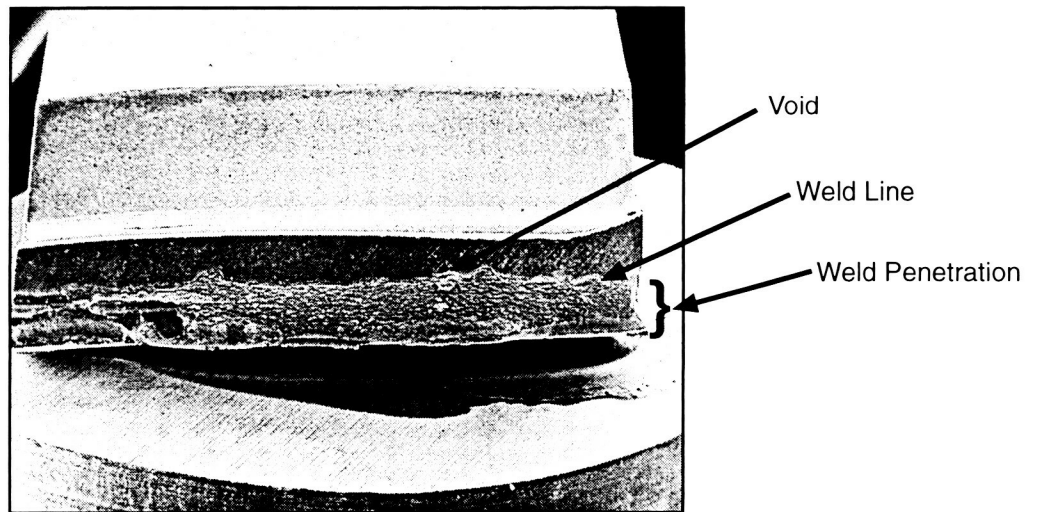


Figure 17. Weld Zone With Prominent Void (12X)

decentering. A run-in test of 10^6 cycles is conducted to eliminate infant mortality. After completing run-in, the pivots are placed in matched sets exhibiting similar decentering patterns.

4. Design a new flex pivot concept.

The fully developed design is a "multi-spoke" configuration machined out of one piece of material, eliminating weld problems. System alignment is improved by ensuring pivot concentricity through one piece construction. The additional blades increase radial and torsional stiffness and provide more load carrying capacity. Final polishing produces blades that are without cracks or flaws and have minimal surface roughness. Pivot fatigue life and therefore system reliability increase as a result. The new flex pivot also improves system pointing accuracy by reducing geometric decentering. Better overall scanner system performance will be achieved through use of the new Ball flex pivot. Figure 18 is a photograph of the pre-polished pivot. Ball is currently seeking patents for this design.

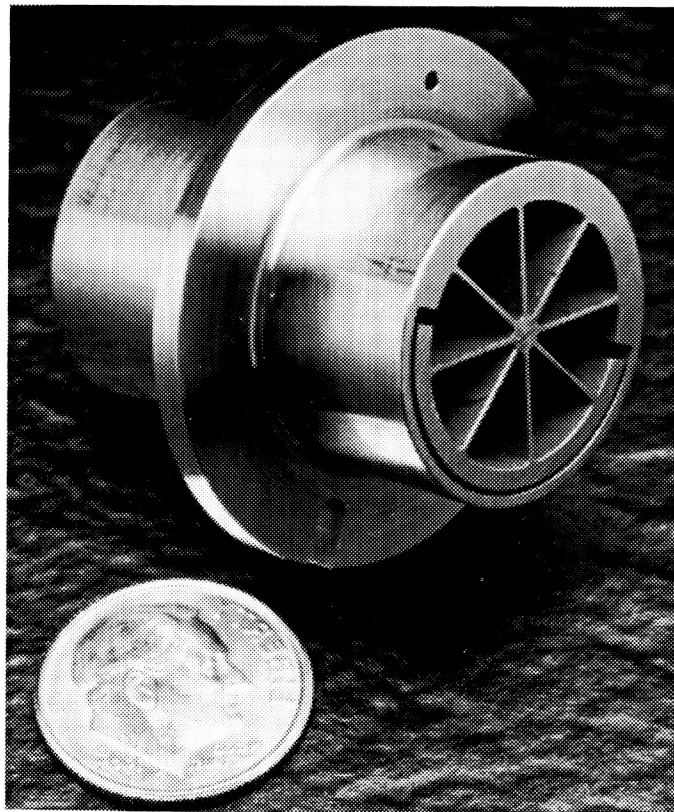


Figure 18. Pre-Polished Pivot

5.0 Program Status

The program was originally contracted to be worked in three phases. The first phase was to include an electronics breadboard and mechanical design development. The second phase was to include a proto-flight qualifying model and the third phase was to construct the flight acceptance model. The project is now in the final phase with an

additional effort added to the contract. Due to some failures and discoveries, discussed in Section 4.0, the second phase model has been returned to have the upgraded hardware and design changes incorporated and re-tested. The flight model, the third phase, has had the new design incorporated and the hardware is almost 100% fabricated.

One of the new flex pivot designs being developed by Ball is a leading contender for incorporation into the mechanism. Development pivots have been manufactured and have successfully passed extensive selection criteria. Ball is now fabricating 30 flight pivots.

6.0 References

1. Seelig, F. A. "*Flexural Pivots for Space Application.*" Bendix Corporation Fluid Power Division, Utica, NY, presented at the 3rd Aerospace Mechanisms Symposium.
2. Olson, J. L. "*The Evaluation of Flexural Pivots to Meet Critical Performance and Life Requirements.*" American Society of Mechanical Engineers, presented at the Design Engineering Conference & Show May 11-14, 1970.

7.0 Acknowledgments

Thanks to Dick Maxwell for his funding and support of this paper. Thanks to the entire TIR team for their support throughout the course of this project.